

Seismic wave propagation in anisotropic ice – Part 1

A. Diez and O. Eisen

Seismic wave propagation in anisotropic ice – Part 1: Elasticity tensor and derived quantities from ice-core properties

A. Diez^{1,2,*} and O. Eisen¹

¹Alfred Wegener Institute Helmholtz Centre for Polar and Marine Research, Bremerhaven, Germany

²Karlsruhe Institute of Technology, Karlsruhe, Germany

*Invited contribution by A. Diez, recipient of the EGU Outstanding Student Poster Award 2014.

Received: 26 May 2014 – Accepted: 9 July 2014 – Published: 4 August 2014

Correspondence to: A. Diez (anja.diez@awi.de)

Published by Copernicus Publications on behalf of the European Geosciences Union.

Title Page

Abstract

Introduction

Conclusions

References

Tables

Figures



Back

Close

Full Screen / Esc

Printer-friendly Version

Interactive Discussion



Abstract

A preferred orientation of the anisotropic ice crystals influences the viscosity of the ice bulk and the dynamic behaviour of glaciers and ice sheets. Knowledge about the distribution of crystal anisotropy, to understand its contribution to ice dynamics, is mainly provided by crystal orientation fabric (COF) data from ice cores. However, the developed anisotropic fabric does not only influence the flow behaviour of ice, but also the propagation of seismic waves. Two effects are important: (i) sudden changes in COF lead to englacial reflections and (ii) the anisotropic fabric induces an angle dependency on the seismic velocities and, thus, also recorded traveltimes. A framework is presented here to connect COF data with the elasticity tensor to determine seismic velocities and reflection coefficients for cone and girdle fabrics from ice-core data. We connect the microscopic anisotropy of the crystals with the macroscopic anisotropy of the ice mass, observable with seismic methods. Elasticity tensors for different fabrics are calculated and used to investigate the influence of the anisotropic ice fabric on seismic velocities and reflection coefficients, englacially as well as for the ice-bed contact. Our work, therefore, provides a contribution to remotely determine the state of bulk ice anisotropy.

1 Introduction

Understanding the dynamic properties of glaciers and ice sheets is one important step to determine past and future behaviour of ice masses. One essential part is to increase our knowledge of the flow of the ice itself. When the ice mass is frozen to the base its flow is primarily determined by internal deformation. The degree thereof is governed by the viscosity (or the inverse of softness) of ice. The viscosity depends on different factors, such as temperature, impurity content and the orientation of the anisotropic ice crystals (Cuffey and Paterson, 2010).

Seismic wave propagation in anisotropic ice – Part 1

A. Diez and O. Eisen

Title Page

Abstract

Introduction

Conclusions

References

Tables

Figures



Back

Close

Full Screen / Esc

Printer-friendly Version

Interactive Discussion



Seismic wave propagation in anisotropic ice – Part 1

A. Diez and O. Eisen

Title Page

Abstract

Introduction

Conclusions

References

Tables

Figures

⏪

⏩

◀

▶

Back

Close

Full Screen / Esc

Printer-friendly Version

Interactive Discussion



Ice is a hexagonal crystal (ice Ih) under natural conditions on earth. These ice crystals can align in specific directions in response to the stresses within an ice mass. In contrast to a random distribution of the ice crystals a preferred orientation causes the complete fabric to be anisotropic. This fabric anisotropy influences the viscosity of the ice, as shear strength is several orders of magnitude smaller perpendicular to the ice crystal's c-axis than parallel to it (Ashby and Duval, 1985; Cuffey and Paterson, 2010).

The influence of anisotropic ice fabric onto the flow behaviour of ice can directly be observed in radar profiles from ice domes. At ice domes and divides a prominent feature of flow conditions is a so called Raymond bump (Raymond, 1983; Martín et al., 2009b). As ice is a non-Newtonian fluid, it is softer and deforms more easily on the flanks of the ice dome or divide due to the higher deviatoric stress there compared to the centre of the dome. Thus, the vertical flow is slower at the dome itself than on the flanks. This leads to an upwarping of the isochronous layers. The development and influence of anisotropic fabric on the flow of ice at divides and the effects on the development of Raymond bumps were, for instance, investigated by Pettit et al. (2007) and Martín et al. (2009a). Often observed features in radar profiles at these Raymond bumps are double bumps and synclines at the flanks (Drews et al., 2013). Martín et al. (2009a) could reproduce these features by including anisotropic rheology into a full-Stokes model. Hence, they are presently considered a direct evidence of the existence of a developed anisotropic fabric, with changes both vertically and laterally, and its influence on the flow behaviour of ice.

A second prominent feature in radar data is the basal layer. Before the advent of multi-static, phase-sensitive radar systems, the basal layer has usually been observed only as an echo-free zone (EFZ). The onset of it was connected to the appearance of folds in ice cores on a centimetre scale (Drews et al., 2009). Considerable progress in radar imaging over the last decade make it now possible to also image the very bottom layer of ice sheets (Bell et al., 2011; NEEM community members, 2013). The now emergent features show an often fuzzy basal layer, with a rough upper surface and considerably disturbed coherency of radar return power. The presence of the basal

Seismic wave propagation in anisotropic ice – Part 1

A. Diez and O. Eisen

Title Page

Abstract

Introduction

Conclusions

References

Tables

Figures

◀

▶

◀

▶

Back

Close

Full Screen / Esc

Printer-friendly Version

Interactive Discussion



layer turns out to be widespread, especially in Antarctica (CReSIS, P. Gogineni, personal communication 2014). As the basal ice near the bed is subject to higher stresses and higher temperatures than the ice above, it is the region where ice physical properties on the microscale change quickest (Faria et al., 2014b). These include changes in crystal orientation fabric (COF) properties and distribution.

With increasing computational power the incorporation of anisotropy into ice flow models becomes feasible in three dimensions as well as on regional scales. However, to include anisotropy into ice-flow modelling we need to understand the development and the distribution of the anisotropic fabric, i.e. we have to observe the variation in the COF distribution over depth, as well as their lateral extent. To extend our ability to determine the influence of these properties on ice flow and map them laterally beyond the 10 cm scale of ice cores, we have to advance our knowledge between the connection of microscale properties and macroscale features on the 10 to 100 meter-scale of geophysical methods like radar and seismics.

The standard method to measure the COF distribution is by analysing thin sections from ice cores under polarized light. The anisotropy is then normally given in form of the sample-averaging eigenvalues of the orientation tensor (Woodcock, 1977) in discrete depth intervals. From this we gain information about the local anisotropic conditions at the ice-core location. Next to the analysis of ice cores, radar data has been used to analyse the changing COF over depth (Matsuoka et al., 2003; Fujita et al., 2006; Eisen et al., 2007; Matsuoka et al., 2009). The challenge in analysing radar data is to distinguish the COF-induced reflections from the numerous conductivity-induced reflections. This distinction is important as conductivity-induced layers are isochrones. By following conductivity-induced reflections in radar data, layers of equal age can be followed over large distances. Currently, identifying and tracing undisturbed layering is one of the major approaches to identify the location of a site for a potentially 1.5 Ma old ice core in East Antarctica (Fischer et al., 2013).

Another possibility to investigate the anisotropic ice fabric on the macroscale can be achieved by analysing COF-induced reflections and traveltimes from seismic data. Not

Seismic wave propagation in anisotropic ice – Part 1

A. Diez and O. Eisen

Title Page

Abstract

Introduction

Conclusions

References

Tables

Figures



Back

Close

Full Screen / Esc

Printer-friendly Version

Interactive Discussion



only the longitudinal (P) pressure waves can be analysed here for the anisotropic fabric but also the transversal waves, i.e. the horizontal (SH) and vertical (SV) shear wave. One of the first studies of seismic anisotropy in context of ice crystal anisotropy was the PhD thesis of Bennett (1988), who derived equations for the calculation of seismic velocities for solid cone and surface cone fabrics. He fitted curves to the slowness surface (inverse of the phase velocity) calculated from an elasticity tensor measured by means of ultrasonic sounding. This was applied to data from Dome C, Antarctica, by Blankenship and Bentley (1987). Bentley (1972) investigated the anisotropic ice fabric at Byrd Station, Antarctica, for which he used ultrasonic logging. To determine the anisotropic seismic velocities for different cone fabrics, he calculated an average from the single crystal velocity for the encountered directions. This approach was used later by Gusmeroli et al. (2012) for analysing the crystal anisotropy from borehole sonic logging at Dome C, Antarctica.

These methods have one shortcoming. They limit the analysis of anisotropy from seismic waves to the analysis of the traveltimes, i.e. seismic velocities. The influence of anisotropy has not only been observed in seismic velocities, but englacial reflections were observed as well in seismic data from Antarctica (Horgan et al., 2011; Hofstede et al., 2013) and Greenland (Horgan et al., 2008). These reflections were interpreted as arising from an abrupt change in fabric orientation. However, to analyse the reflection signature and determine the actual change in COF, we first need an understanding of the reflection coefficient for changing incoming angles for the transition between different anisotropic fabrics.

One way to improve the analysis of seismic data is to apply full waveform inversion algorithms, i.e. the analysis of the complete observed wave field and not only parts of it like reflections or traveltimes, which gains more and more importance in applied geophysics in general. If we want to be able to investigate and understand the influence of the anisotropic ice fabric on the seismic wave field and develop possibilities to derive information from traveltimes and reflection signatures about different anisotropic ice

fabrics from seismic data, we need to be able to derive the elasticity tensor for different COF distributions.

In this paper we extend the analysis of seismic velocities beyond cone fabrics and derive the elasticity tensor, which is necessary to describe the seismic wavefield in anisotropic media. The description of seismic wave propagation in anisotropic materials is based on the elasticity tensor, a 4th order tensor with 21 unknowns in the general case of anisotropy. If the elasticity tensor is known, seismic velocities, reflection coefficient or reflection angles can be calculated. From ice core analysis one normally gains the COF eigenvalues describing the distribution of the crystal orientations. Hence, we first need a connection between the COF eigenvalues and the elasticity tensor.

We present a framework here to derive the elasticity tensor from the COF eigenvalues for cone as well as different girdle fabrics. We derive opening angles for the enveloping of the c-axis distribution from the COF eigenvalues. We then integrate using a monocrystal elasticity tensor for these derived distributions to obtain the elasticity tensor for the different anisotropic fabrics (Sect. 3). Based on these derived elasticity tensors we calculate seismic velocities and reflection coefficients for different c-axes distributions. As examples, we investigate the compressional wave velocity variations with increasing angle for different fabrics and the reflection coefficients for a change from isotropic to girdle fabric for compressional and shear waves. Further, we analyse the influence of anisotropy on the reflection signature of the ice–bed interface and discuss these results in Sect. 4. This is the first part of two companion papers. The calculations introduced here will be applied to ice-core and seismic data from Kohnen station, Antarctica in Part 2, Diez et al. (2014).

2 Ice crystal anisotropy

The ice crystal is an anisotropic, hexagonal crystal with the basal plane perpendicular to the ice crystal's c-axis. Due to the existing stresses within glaciers and ice sheets these anisotropic ice crystals can be forced to align in one or several specific directions.

Seismic wave propagation in anisotropic ice – Part 1

A. Diez and O. Eisen

Title Page

Abstract

Introduction

Conclusions

References

Tables

Figures



Back

Close

Full Screen / Esc

Printer-friendly Version

Interactive Discussion



In such cases the crystal's c-axis is oriented perpendicular to the main direction of stress (Cuffey and Paterson, 2010). Depending on the stress regime different COF distributions develop (Fig. 1).

Different fabric distributions were discussed by Wallbrecher (1986), who classifies 8 different fabric groups. Three of which we will use in the following analysis of the influence of ice crystal anisotropy on seismic wave propagation: (i) the cluster distribution, (ii) the thick girdle distribution, and (iii) the partial girdle distribution. These distributions are shown in Fig. 1. The sketches show the enveloping of the specific c-axes distribution for the different fabrics. Here, the isotropic case is part of the cluster distribution. The most extreme form of anisotropy we can expect in ice is a vertical single maximum (VSM) fabric, where all ice crystals are oriented vertical. Note that the term "lattice-preferred orientation (LPO)" is used as well to refer to the orientation of the crystals (Faria et al., 2014a), in addition to COF.

2.1 Crystal orientation fabric measurements

The standard method of measuring COF distributions is by analysing thin sections from ice cores under polarized light using an automatic fabric analyser (Wilson et al., 2003; Peternell et al., 2010). The c-axis orientation of each single crystal is determined and can be given as a unit vector (c). These orientations can be presented in Schmidt plots, an equal-area projection of a sphere onto a plane, or as eigenvalues $\lambda_1, \lambda_2, \lambda_3$ of the weighted orientation tensor

$$A_{ij} = W \sum_{l=1}^n (c_l c_l)_i, \quad \text{with } i, j = 1, 2, 3. \quad (1)$$

The number of grains is given by n and W is a weighting function, with weighting, e.g. by grain number ($W = 1/n$) or by area. The three eigenvalues, with $\lambda_1 \leq \lambda_2 \leq \lambda_3$ and $\sum \lambda_i = 1$, determine the extension of a rotation ellipsoid. The corresponding eigenvectors cannot be given, when the orientation of the ice core within the borehole is not

Seismic wave propagation in anisotropic ice – Part 1

A. Diez and O. Eisen

Title Page

Abstract

Introduction

Conclusions

References

Tables

Figures

◀

▶

◀

▶

Back

Close

Full Screen / Esc

Printer-friendly Version

Interactive Discussion



measured in geolocated coordinates. Hence, the direction to which these eigenvalues apply is often unknown.

Another possibility to describe the anisotropic fabric is to calculate the spherical aperture from the orientation tensor. Hence, the c-axis distribution is given in form of one opening angle for the enveloping cone (Wallbrecher, 1986). However, this limits the analysis of anisotropy to cone fabrics.

For the following derivation of the elasticity tensor we will use two opening angles for the description of the enveloping of the c-axis distribution. Thus, we are able to take into account cone as well as girdle fabric distributions. We distinguish between an opening angle χ in x_1 -direction and an opening angle φ in x_2 -direction in a coordinate system where the x_3 -axis is pointing downwards (Fig. 1). These opening angles will be calculated from the COF eigenvalues for the analysis of seismic wave propagation (Sect. 3.1).

The two opening angles determine the kind of fabric (Fig. 1). If the angles φ and χ are equal, the c-axis distribution is a cluster or cone distribution with the cone opening angle $\varphi = \chi$. The two extrema of this distribution are the uniform distributions, i.e. the isotropic case and the VSM-fabric. All ice crystals are oriented vertically in case of a VSM-fabric. The eigenvalues are $\lambda_1 = \lambda_2 = 0$ and $\lambda_3 = 1$ and the cone opening angle is 0° . The ice crystals are randomly oriented in case of isotropic fabric. The eigenvalues are then $\lambda_1 = \lambda_2 = \lambda_3 = 1/3$ and the cone opening angle is 90° . The thick girdle fabric is a distribution where the c-axes are distributed between two planes with a certain distance, so that the opening angle φ in x_2 -direction is 90° and χ in x_1 -direction gives the thickness of the girdle. The partial girdle fabric is a distribution where all ice crystal c-axes are in one plane, but only within a slice of this plane, so that the opening angle χ in x_1 -direction is 0° and φ in x_2 -direction gives the size of the slice within the plane. A girdle fabric with $\chi = 0^\circ$ and $\varphi = 90^\circ$ would correspond to the eigenvalues $\lambda_1 = 0$ and $\lambda_2 = \lambda_3 = 0.5$.

Seismic wave propagation in anisotropic ice – Part 1

A. Diez and O. Eisen

[Title Page](#)[Abstract](#)[Introduction](#)[Conclusions](#)[References](#)[Tables](#)[Figures](#)[◀](#)[▶](#)[◀](#)[▶](#)[Back](#)[Close](#)[Full Screen / Esc](#)[Printer-friendly Version](#)[Interactive Discussion](#)

2.2 Seismic anisotropy

The wave propagation of seismic waves is influenced by the anisotropic material, effecting, e.g. seismic velocities, reflection coefficients and reflection angles, among other properties. The propagation of wavefronts in the anisotropic case is no longer spherical. Figure 2 shows the anisotropic wavefront for a P-wave travelling in a VSM-fabric (red line) and the spherical wavefront for a P-wave in isotropic ice fabric (dashed black line). For the anisotropic case group and phase velocity, as well as group angle θ and phase angle ϑ , are no longer the same. The group velocity determines the traveltime. The phase velocity vector is normal to the wavefront. Thus, the phase velocity and phase angle ϑ are needed for the calculation of reflection and transmission angles as well as reflection coefficients.

For an anisotropic medium the linear relationship between tensors of stress σ_{mn} and strain τ_{mn} is described by Hook's law

$$\sigma_{mn} = c_{mnop} \tau_{op}, \quad (2)$$

with the elasticity tensor c_{mnop} and $m, n, o, p = 1, 2, 3$. In the isotropic case these 81 components of the elasticity tensor can be reduced to the two well-known Lamé parameters. In the general anisotropic case, symmetry consideration of strain and stress tensor apply, as well as thermodynamic consideration (Aki and Richards, 2002). Hence, the general anisotropic elasticity tensor consist of 21 independent components and is referred to as triclinic.

To determine seismic velocities in anisotropic media a solution for the wave equation needs to be found. Given here is the wave equation for homogeneous, linear elastic media, without external forces and with triclinic anisotropy

$$\rho \frac{\partial^2 u_m}{\partial t^2} - c_{mnop} \frac{\partial^2 u_o}{\partial x_n \partial x_p} = 0, \quad (3)$$

with ρ the density of the material, t time, the components u_m and u_o of the displacement vector \mathbf{u} and the different spatial directions x_n, x_p . Solving this equation leads

to an eigenvalue problem, the so called Christoffel equation. For a detailed derivation see, e.g. Tsvankin (2001).

Finally, three non-trivial solutions exist for this eigenvalue problem, giving the three phase velocities and vectors for the quasi compressional (qP), the quasi vertical (qSV) and the quasi horizontal shear (qSH) wave. The phase vectors are orthogonal to each other. However, qP- and qSV-waves are coupled, so the waves are not necessarily pure longitudinal or shear waves outside of the symmetry planes. Therefore, they are additionally denoted as “quasi” waves, i.e. qP-, qSV- and qSH-waves. As the following analyses are mostly within the symmetry planes the waves will from now on be denoted as P-, SV- and SH-waves. Nevertheless, outside of the symmetry planes this term is not strictly correct.

To be able to find analytical solutions of the Christoffel matrix the anisotropic materials are distinguished by their different symmetries. Additionally, to simplify calculations with the elasticity tensor we will use the compressed Voigt notation (Voigt, 1910) for the elasticity tensor $c_{mnop} \rightarrow C_{ij}$. Therefore, the index combinations of mn and op are replaced by indices between 1 and 6 ($11 \equiv 1$, $22 \equiv 2$, $33 \equiv 3$, $23 \equiv 4$, $13 \equiv 5$, $12 \equiv 6$). Considering only certain symmetries reduces the unknowns of the elasticity tensor C_{ij} further. For the analysis of anisotropic ice we consider cone, thick and partial girdle fabric. Partial girdle fabric is the fabric with the lowest symmetry, corresponding to an orthorhombic medium, with 9 unknowns,

$$C_{ij} = \begin{pmatrix} C_{11} & C_{12} & C_{13} & 0 & 0 & 0 \\ C_{12} & C_{22} & C_{23} & 0 & 0 & 0 \\ C_{13} & C_{23} & C_{33} & 0 & 0 & 0 \\ 0 & 0 & 0 & C_{44} & 0 & 0 \\ 0 & 0 & 0 & 0 & C_{55} & 0 \\ 0 & 0 & 0 & 0 & 0 & C_{66} \end{pmatrix}. \quad (4)$$

In case of orthorhombic media three symmetry planes, i.e. orthogonal planes of mirror symmetry exist. The number of unknowns can be reduced further to five unknowns if

Seismic wave propagation in anisotropic ice – Part 1

A. Diez and O. Eisen

Title Page	
Abstract	Introduction
Conclusions	References
Tables	Figures
◀	▶
◀	▶
Back	Close
Full Screen / Esc	
Printer-friendly Version	
Interactive Discussion	



Seismic wave propagation in anisotropic ice – Part 1

A. Diez and O. Eisen

Title Page

Abstract

Introduction

Conclusions

References

Tables

Figures

⏪

⏩

◀

▶

Back

Close

Full Screen / Esc

Printer-friendly Version

Interactive Discussion



transversely isotropic media exist, resulting in an anisotropy with a single axis of rotation symmetry. This is normally distinguished in vertical transversely isotropic (VTI) and horizontal transversely isotropic (HTI) media, with a vertical and horizontal axis of rotation symmetry, respectively. A vertical cone fabric would be classified as VTI media while a thick girdle fabric as given in Fig. 1 would be classified as HTI media. This distinction is important for the calculation of seismic velocities and reflection coefficients as the calculation simplifies for wave propagation within symmetry planes of the anisotropic fabric (Sect. 4)

3 Calculation of elasticity tensor from COF eigenvalues

From the analysis of ice cores we gain the COF eigenvalues describing the crystal anisotropy over depth. The propagation of seismic waves in anisotropic media can be calculated from the elasticity tensor. Hence, a relationship between the COF eigenvalues and the elasticity tensor is needed.

We will use a measured monocrystal elasticity tensor here to calculate the elasticity tensor for the different observed anisotropic fabrics in ice from the COF eigenvalues. For monocrystalline ice the components of the elasticity tensor have been measured by a number of authors with different methods. The choice of the elasticity tensor will be investigated in more detail in Part 2, Diez et al. (2014), where we find best agreement between measured and calculated velocities using the elasticity tensor of Gammon et al. (1983) ($C_{11} = 13.93 \pm 0.04 \text{ GN m}^{-2}$; $C_{33} = 15.01 \pm 0.05 \text{ GN m}^{-2}$; $C_{55} = 3.01 \pm 0.01 \text{ GN m}^{-2}$; $C_{12} = 7.08 \pm 0.04 \text{ GN m}^{-2}$; $C_{13} = 5.77 \pm 0.02 \text{ GN m}^{-2}$). Hence, we will use this elasticity tensor in the following calculations. The c-axis of this ice crystal is oriented vertically here, parallel to the x_3 -direction (Fig. 1).

3.1 From COF eigenvalues to opening angles

When the COF eigenvalues are derived, the information on the fabric distribution is significantly reduced, especially as the corresponding eigenvectors are normally unknown. Hence, it is not possible to determine the elasticity tensor with at least five unknowns directly from the three COF eigenvalues. Therefore, we first subdivide the observed anisotropies into different fabric groups (cone, thick girdle and partial girdle fabric) by means of the eigenvalues and afterwards determine their opening angles (Sect. 2.1).

To differentiate between cone and girdle fabric Woodcock (1977) suggests a logarithmic representation of the eigenvalues and classification by a slope

$$m = \frac{\ln(\lambda_3/\lambda_2)}{\ln(\lambda_2/\lambda_1)}. \quad (5)$$

The fabric is a cone fabric with $m > 1$ and a girdle fabric with $m < 1$. However, we want to put a stronger tendency towards a classification of the fabric as cone fabric. In the seismic sense a cone fabric is a VTI media. It is easier to calculate velocities and reflection coefficients for VTI media compared to girdle fabric, i.e. HTI media. Hence, we use a threshold value to distinguish between cone and girdle fabric. If $\lambda_1 \leq 0.1$ and $\lambda_2 \geq 0.2$ the fabric is classified as girdle fabric, everything else is classified as cone fabric. Additionally, we set a threshold to distinguish within the girdle fabric between partial and thick girdle fabric. If $\lambda_1 \leq 0.05$ the fabric is classified as partial girdle, otherwise as thick girdle. By distinguishing between these fabrics we know, that $\varphi = \chi$ for the cone fabric, $\varphi = 90^\circ$ for the thick girdle fabric and $\chi = 90^\circ$ for the partial girdle fabric (Fig. 1).

In the next step the remaining, unknown opening angle for the different fabrics needs to be calculated from the eigenvalues, i.e. φ for the cone fabric, χ for the thick girdle fabric and φ for the partial girdle fabric. Wallbrecher (1986) for instance connects the opening angle φ of a cone fabric with the eigenvalue λ_3 by $\lambda_3 = 1 - 2/3 \sin^2 \varphi$. To verify this calculation the eigenvalues for cone angles between 0 and 90° were calculated.

tensor S_{mnop} of a crystal is the inverse of the elasticity tensor, here given in terms of Hook's law (Eq. 2):

$$\tau_{mn} = S_{mnop}\sigma_{op}. \quad (6)$$

5 For the inversion of elasticity to compliance tensor and vice versa see, e.g. Bower (2010). The method of Voigt (1910) and Reuss (1929) is an approximation of the elasticity tensor due to violation of local equilibrium and compatibility conditions across grain boundaries, respectively. Hill (1952) showed that the concepts of Voigt (1910) and of Reuss (1929) give the upper and lower limit for the elastic moduli of the poly-
10 crystal C_{ij} , referred to as Voigt–Reuss bounds,

$$C_{ij}^R \leq C_{ij} \leq C_{ij}^V, \quad (7)$$

where the superscripts R and V denote Reuss (1929) and Voigt (1910) calculation, respectively.

15 To obtain the elasticity tensor of the anisotropic polycrystal C_{ij} from the elasticity tensor of the monocrystal C_{ij}^m with different orientations one has to integrate the elasticity tensor $\tilde{C}_{ij}^m(\phi)$ with a probability density function $F(\phi)$ for the different c-axes orientations, where ϕ gives the minimum (ϕ_1) and maximum (ϕ_2) extent of the c-axes in the plane. This plane is perpendicular to the corresponding rotation axis, so that the elasticity tensor $\tilde{C}_{ij}^m(\phi)$ is determined from the monocrystal elasticity tensor C_{ij}^m using the
20 rotation matrix R_{ij}^C

$$\tilde{C}_{ij}^m(\phi) = (R_{ij}^C)^T C_{ij}^m R_{ij}^C. \quad (8)$$

The rotation matrices R_{ij}^C for the different directions in space are given in Appendix A2, $(R_{ij}^C)^T$ is the transposed of R_{ij}^C . The same applies for the calculation of the monocrystal compliance tensor depending on ϕ , with
25

$$\tilde{S}_{ij}^m(\phi) = (R_{ij}^S)^T S_{ij}^m R_{ij}^S. \quad (9)$$

Seismic wave propagation in anisotropic ice – Part 1

A. Diez and O. Eisen

Title Page	
Abstract	Introduction
Conclusions	References
Tables	Figures
◀	▶
◀	▶
Back	Close
Full Screen / Esc	
Printer-friendly Version	
Interactive Discussion	



with the rotation matrix R_{ij}^S for the compliance tensor (Appendix A2) and its transposed $(R_{ij}^S)^T$. For a uniform distribution of the c-axis orientations the probability density function can be given by

$$F(\phi) = \frac{1}{\phi_2 - \phi_1} \quad \text{for } \phi_1 \leq \phi \leq \phi_2 \quad (10)$$

$$= 0 \quad \text{for } \phi_2 \leq \phi \leq \pi; -\pi \leq \phi \leq \phi_1, \quad (11)$$

which is symmetric around the main orientation, so that $\phi_1 = -\phi_0$ and $\phi_2 = +\phi_0$. The elasticity tensor of the anisotropic polycrystal is then calculated by

$$C_{ij} = \frac{1}{2\phi_0} \int_{-\phi_0}^{+\phi_0} \tilde{C}_{ij}^m(\phi) d\phi, \quad (12)$$

and the compliance tensor is calculated by

$$S_{ij} = \frac{1}{2\phi_0} \int_{-\phi_0}^{+\phi_0} \tilde{S}_{ij}^m(\phi) d\phi. \quad (13)$$

After considering the orthorhombic symmetry and some rearranging of the results of Eqs. (12) and (13) the components of the elasticity tensor and compliance tensor of a polycrystal can be expressed in compact form. The results are different here, for c-axes distributions in the different spatial directions x_1 , x_2 and x_3 . As an example, the equations for the elasticity and compliance tensor for a rotation around the x_1 direction are given in Appendix A3. This would correspond to a c-axis distribution in the $[x_2, x_3]$ -plane. The equations for rotation around the x_2 -axis and the x_3 -axis can equally be derived from Eqs. (12) and (13).

Seismic wave propagation in anisotropic ice – Part 1

A. Diez and O. Eisen

Title Page

Abstract

Introduction

Conclusions

References

Tables

Figures

◀

▶

◀

▶

Back

Close

Full Screen / Esc

Printer-friendly Version

Interactive Discussion



The different rotation directions to calculate the polycrystal elasticity tensor C_{ij} from a vertically oriented monocrystal elasticity tensor C_{ij}^m for cone, thick girdle and partial girdle fabric are listed in Table 1. They are as well valid for the compliance tensor. For the calculation of the elasticity tensor of a partial girdle (Fig. 1) the elasticity tensor of the monocrystal C_{ij}^m is rotated around the x_1 -axis with the opening angle of the partial girdle in x_2 -direction (φ). The elasticity tensor is then calculated using Eq. (A12) with $\phi_0 = \varphi$. For a thick girdle $\varphi = 90^\circ$ to gain a full girdle in the $[x_2, x_3]$ -plane in the first step. In a second step this elasticity tensor obtained for a full girdle is then rotated around the x_2 -axis with $\phi_0 = \chi$. For cone fabrics with different opening angles the elasticity tensor of a monocrystal is rotated around the x_1 -axis (Eq. A12) in a first step using the cone opening angle ($\phi_0 = \varphi = \chi$) and, afterwards, the obtained elasticity tensor is rotated around the x_3 -axis with $\phi_0 = 90^\circ$.

3.3 Limitations of the method

Nanthikesan and Sunder (1994) developed the approach to calculate the polycrystal elasticity tensor from the monocrystal elasticity tensors for, what they call, S1 (vertical single maximum), S2 (horizontal girdle) and S3 (horizontal partial girdle) ice for given opening angles. They found that the Voigt–Reuss bounds for these fabrics are within 4.2% of each other and concluded from this that either calculation, by means of the elasticity tensor (Eq. 12) or compliance tensor (Eq. 13), can be used to calculate the elasticity tensor of the polycrystal. We use the approach of Nanthikesan and Sunder (1994) not only for the calculation of partial girdle fabrics but also for the calculation of the polycrystal elasticity tensor of thick girdle and cone fabrics.

By comparing the individual components of the elasticity tensor derived following Voigt (1910) (Eq. 12) with those of the elasticity tensor derived following Reuss (1929) (Eq. 13 and taking the inverse of the compliance tensor) the largest difference of 4.2% for all the investigated fabrics can be found for the components C_{44} (S_{44}) of a partial girdle with an opening angle of 50° and 90° . Thus, for all fabrics in this study, the Voigt–Reuss bounds are within 4.2% of each other and we follow Nanthikesan and

Sunder (1994) in their argumentation that either calculation can be used. However, using the Voigt (1910) calculation no extra step in the calculation is needed to invert the compliance tensor. Therefore, for all further calculations the approach by Voigt (1910) is used (Eq. 12).

For the calculation of the anisotropic polycrystal from the monocrystal neither grain size nor grain boundaries are considered. Elvin (1996) investigated the number of grains that are necessary to homogenize the elastic properties of polycrystalline ice and found, that at least 230 grains are needed for girdle fabric (S2 ice). This number of ice crystals should be reached with seismic waves in ice of around 300 Hz, i.e. a wavelength of more than 10 m and ice crystals with ≤ 0.1 m diameter on average. Additionally, Elvin (1996) considered two cases, with and without grain boundary sliding. In absence of grain-boundary sliding the anisotropy mainly defines the elastic behaviour. Otherwise, grain shape and grain-boundary sliding become important as well. A certain mistake is, thus, made for the calculation of the polycrystal by only considering the influence of the anisotropy of the monocrystal.

The resultant polycrystal elasticity tensors depends of course on the choice of the monocrystal elasticity tensor. Different authors (Jona and Scherrer, 1952; Green and Mackinnen, 1956; Bass et al., 1957; Brockamp and Querfurth, 1964; Bennett, 1988; Dantl, 1968; Gammon et al., 1983) measured and calculated (Penny, 1948) the monocrystal elasticity tensor. A comparison of the different elasticity tensors used can be found in Part 2 (Diez et al., 2014). There we investigate results of a vertical seismic profiling survey in comparison to quantities from measured COF eigenvalues. We find the best agreement between measured and calculated velocities using the monocrystal elasticity tensor of Gammon et al. (1983) for the derivation of the polycrystal elasticity tensor.

Seismic wave propagation in anisotropic ice – Part 1

A. Diez and O. Eisen

Title Page

Abstract Introduction

Conclusions References

Tables Figures

◀ ▶

◀ ▶

Back Close

Full Screen / Esc

Printer-friendly Version

Interactive Discussion



4 Seismic velocities and reflection coefficients in anisotropic ice

From the derived elasticity tensor we can now calculate velocities and reflection coefficients. Many approximations as well as exact solutions exist for the calculation of velocities and reflection coefficients for different anisotropic fabrics. They are mostly limited to certain symmetries.

In case of the velocities, most studies have been done on VTI media (e.g. Daley and Heron, 1977). These solutions are still valid within the symmetry planes of HTI media. To be able to calculate seismic velocities for the different fabrics in ice we will use a calculation of velocities for orthorhombic media derived by Daley and Krebs (2004) (Sect. 4.1). We compare the velocities calculated based on the derived elasticity tensor with the well known velocities for a solid cone that were derived by Bennett (1988) (Sect. 4.2).

For the calculation of the reflection coefficient we use exact (Graebner, 1992) as well as approximate (Rüger, 1997; Zillmer et al., 1998b) calculations (Sect. 4.3). We show the reflection coefficients for an abrupt change from isotropic to partial girdle fabric here as an example (Sect. 4.4). Additionally, we investigate the influence on the reflection signature of an anisotropic ice mass above the base (Sect. 4.5).

4.1 Velocities in orthorhombic media

For the special case of wave propagation in ice with a developed cone fabric anisotropy Bennett (1988) derived equations of the slowness surface for P-, SV- and SH-waves. The phase velocities are given by the inverse of the slowness surface. To calculate the slowness surface over different angles Bennett (1988) first derived the elasticity tensor from single natural ice crystals by measurements of ultrasonic pulses with 600 kHz. With the derived equations velocities for different incoming angles ϑ in dependence of the cone opening angle φ can be calculated. It is not possible to calculate velocities for girdle fabrics.

Seismic wave propagation in anisotropic ice – Part 1

A. Diez and O. Eisen

Title Page

Abstract

Introduction

Conclusions

References

Tables

Figures

◀

▶

◀

▶

Back

Close

Full Screen / Esc

Printer-friendly Version

Interactive Discussion



Using the derived elasticity tensor we are now able to calculate velocities for different COF distributions. Therefore, we use the equations derived by Daley and Krebs (2004) for the calculation of phase velocities v_{ph} (v_{p} , v_{sv} , v_{sh}) in dependency of the phase angle ϑ for orthorhombic media as given in Appendix B1 (Eqs. B1–B3).

From these phase velocities we have to calculate the group velocities for the calculation of traveltimes. The calculation of the group velocity vector $\mathbf{v}_{\mathbf{g}}$ can be found, e.g. in Rommel and Tsvankin (2000) and Tsvankin (2001). If the propagation of the seismic wave is within symmetry planes of the anisotropic fabric the group velocity and group angle can be given in compact form. The group velocity $v_{\mathbf{g}}$ is then calculated from the phase velocity v_{ph} by

$$v_{\mathbf{g}} = v_{\text{ph}} \sqrt{1 + \left(\frac{1}{v_{\text{ph}}} \frac{\partial v_{\text{ph}}}{\partial \vartheta} \right)^2} \quad (14)$$

with the group angle θ in the symmetry plane defined by

$$\tan \theta = \frac{\tan \vartheta + \frac{1}{v_{\text{ph}}} \frac{\partial v_{\text{ph}}}{\partial \vartheta}}{1 - \frac{1}{v_{\text{ph}}} \frac{\partial v_{\text{ph}}}{\partial \vartheta} \tan \vartheta}. \quad (15)$$

Outside the symmetry planes of, e.g. HTI media all components of the group velocity vector $\mathbf{v}_{\mathbf{g}}$ have to be considered (Appendix B1).

Figure 3 shows the phase (dashed curves) and group velocities (solid curves) in dependency of the corresponding phase ϑ and group angle θ of P- (red), SV- (light blue) and SH-waves (blue) for a VSM-fabric. The largest difference between phase and group velocity can be observed for the SV-wave (light blue curves) with a triplication in the group velocity for group angles of 43–47°. Here three different velocities are given for each angle. The SV-wave velocity is largest for 45° incoming angle (phase as well as group angle) with 2180 m s⁻¹, decreasing for 0° and 90° to 1810 m s⁻¹. Variations

for the SH-wave are rather small with velocities increasing between 0° and 90° from 1810 m s^{-1} to 1930 m s^{-1} . The P-wave velocity has a minimum at $\sim 51^\circ$ incoming angle with 3770 m s^{-1} . The highest wave speed is observed for waves parallel to the c-axis of an ice crystal (0° incoming angle) with 4040 m s^{-1} and 150 m s^{-1} slower perpendicular to it.

4.2 Velocities for anisotropic ice

By deriving the elasticity tensor for different fabrics the group and phase velocities of P-, SH- and SV-wave for these fabrics can now be calculated. Figure 4 show the P-wave phase velocity for different cone and girdle fabrics calculated with the equations given in Daley and Krebs (2004) and the equations derived by Bennett (1988) for a solid cone. The phase velocity for the SH- and SV-wave as well as the corresponding group velocities can be displayed accordingly (Diez, 2013). Here, we will limit our analysis to P-waves. However, with the derived elasticity tensor SH- and SV-wave velocities can just as well be investigated and the effect of shear (S)-wave splitting can be analysed.

The subfigure (d) in Fig. 4 shows the velocities calculated from the equations derived by Bennett (1988) for a solid cone from the elasticity tensor he measured at -10°C . These velocities were corrected to -16°C (Kohnen, 1974; Gammon et al., 1983) for better comparison with the other results, where we use the elasticity tensor of Gammon et al. (1983) measured at -16°C . The other subfigures are phase velocities calculated with Eq. (12) from an elasticity tensor derived following the steps in Table 1 with the elasticity tensor measured by Gammon et al. (1983). The top row (Fig. 4) shows velocities for cone fabric (subfigure a: VTI) as well as partial girdle fabric (b: HTI) and thick girdle fabric (c: HTI) in the $[x_2, x_3]$ -plane, while the bottom rows show velocities for cone fabric calculated following Bennett (1988) (d: VTI) as well as partial girdle fabric (f: $\psi = 90^\circ$) and thick girdle fabric (e: $\psi = 90^\circ$) in the $[x_1, x_3]$ -plane.

The partial girdle ($\chi = 0^\circ$, Fig. 4b and e) with $\varphi = 90^\circ$ displays the same fabric as the thick girdle ($\varphi = 90^\circ$, Fig. 4c and f) with $\chi = 0^\circ$. The same applies to the cone fabric with an opening angle of 90° (Fig. 4a and d) as well as the thick girdle fabric ($\varphi = 90^\circ$) with

Seismic wave propagation in anisotropic ice – Part 1

A. Diez and O. Eisen

Title Page

Abstract

Introduction

Conclusions

References

Tables

Figures



Back

Close

Full Screen / Esc

Printer-friendly Version

Interactive Discussion



Seismic wave propagation in anisotropic ice – Part 1

A. Diez and O. Eisen

Title Page

Abstract

Introduction

Conclusions

References

Tables

Figures

◀

▶

◀

▶

Back

Close

Full Screen / Esc

Printer-friendly Version

Interactive Discussion



$\chi = 90^\circ$ (Fig. 4c and f), both showing the isotropic state. Apart from Bennett's velocities, these velocities for the isotropic state (Fig. 4a, c and f) are obviously not isotropic. Slight variations still exist for these velocities with increasing incoming angle. This is due to artefacts that seem to appear from the derivation of the elasticity tensor for the isotropic state using the single crystal elasticity tensor.

It should also be noted, that for a thick girdle with $\varphi = \chi = 90^\circ$ the variations over the incoming angle are just reversed to that of the cone fabric with opening angle $\varphi = \chi = 90^\circ$. This reflects the difference in the calculation of the elasticity tensor from cone fabric and girdle fabric. While a girdle with $\varphi = 90^\circ$ ($\chi = 0^\circ$) is calculated in the first step for both fabrics (Table 1) by integration with rotation around the x_1 -axis, the second step is an integration with rotation around the x_3 -axis for the cone fabric and around the x_2 -axis for the thick girdle fabric.

The higher velocities calculated with the equations of Bennett (1988) (Fig. 4d) are due to the difference in the elasticity tensor as the elasticity tensor derived by Gammon et al. (1983) was used for the calculation in case of the other subfigures (Fig. 4a–c, e and f). The Bennett (1988) calculation exhibits an isotropic state for $\varphi = \chi = 90^\circ$. However, this is only possible as Bennett (1988) used fitted curves for the derivation of the slowness surface.

4.3 Reflection coefficients

The calculation of reflection coefficients for different incoming angles is already rather complicated for layered isotropic media given by the Zoeppritz equations (e.g. Aki and Richards, 2002). In case of anisotropic media most of the studies have been done for VTI media (Keith and Crampin, 1977; Daley and Heron, 1977) and in terms of Thomsen parameters (Thomsen, 1993). A comprehensive overview of the different calculations of reflection coefficients for VTI and HTI media is given by Rüger (2002).

In the following, we use equations derived by Zillmer et al. (1997) by means of perturbation theory for the calculation of englacial reflection horizons. These equations for general anisotropy were simplified by Zillmer et al. (1998a) for weak contrast interfaces.

Seismic wave propagation in anisotropic ice – Part 1

A. Diez and O. Eisen

Title Page

Abstract

Introduction

Conclusions

References

Tables

Figures

◀

▶

◀

▶

Back

Close

Full Screen / Esc

Printer-friendly Version

Interactive Discussion



They are especially practical for the reflection coefficients in ice. For the isotropic reference values the elasticity tensor for isotropic ice can be used and no average needs to be taken over different materials. The reflection coefficients for the anisotropic material are then calculated as perturbation of the isotropic ice fabric. Thus, reflection coefficients for P-, SV- and SH-waves are obtained. The equations for the calculation of reflection coefficients are given in Appendix B2. The R_{shsh} and R_{svsv} reflection coefficients are restricted to a symmetry plane of the layered medium. The indices give the polarisation of the incoming and reflected wave, e.g. R_{pp} is the reflection coefficient for an incoming P-wave, reflected as P-wave, equivalent for R_{shsh} and R_{svsv} .

For the calculation of the reflection coefficient between cone fabric (VTI) and the bed the derivation of Thomsen (1993), further developed by Rüger (1997), for the P-wave reflection coefficient can be used as approximate equations. Exact solutions for VTI media are, for example, given by Keith and Crampin (1977) or Graebner (1992).

4.4 Reflection coefficients for anisotropic ice

With the equations given in Appendix B2 (Zillmer et al., 1998a) reflection coefficients can be calculated for different fabric transitions. A large amount of transitions between different anisotropic ice fabrics is possible here. Figure 5 shows as an example the R_{pp} , R_{shsh} and R_{svsv} reflection coefficient for the transition at a layer interface from an isotropic fabric to a partial girdle fabric, both for HTI media ($\psi = 0^\circ$) and with an azimuth of $\psi = 90^\circ$.

The reflection coefficients are given for angles of incidence between 0° and 60° . This has two reasons. Firstly, most seismic surveys do not exceed an incoming angle of 60° as this already corresponds to a large offset compared to the probed depth. Secondly and more important, the calculation of the reflection coefficients using Eqs. (B12)–(B13) is not exact. Instead, the error increases with increasing incoming angle.

The largest magnitude of reflection coefficients can be observed for the SVSV-reflection (Fig. 5). However, the reflection coefficients are ≤ 0.1 for all fabric combinations shown here. Especially for the PP-reflection the reflection coefficients between

Seismic wave propagation in anisotropic ice – Part 1

A. Diez and O. Eisen

[Title Page](#)[Abstract](#)[Introduction](#)[Conclusions](#)[References](#)[Tables](#)[Figures](#)[◀](#)[▶](#)[◀](#)[▶](#)[Back](#)[Close](#)[Full Screen / Esc](#)[Printer-friendly Version](#)[Interactive Discussion](#)

different anisotropic fabrics are small. The PP-reflection between, e.g. isotropic and VSM-fabric ice for normal incident is < 0.02 . For comparison the reflection coefficient between isotropic and lithified sediments (Fig. 6) is ~ 0.4 . Hence, reflection coefficients at the ice–bed interface are an order of magnitude larger than reflection coefficients for the transition between different anisotropic fabrics. To be able to observe englacial seismic reflections abrupt changes (i.e. within a wavelength) with significant variations in the orientation of the ice crystals are needed. Such englacial reflections have been observed in data from Greenland (Horgan et al., 2008), Antarctica (Horgan et al., 2011; Hofstede et al., 2013) but also in the Swiss Alps (Polom et al., 2014; Diez et al., 2013). These reflections can indicate a change in the anisotropic fabric. However, the investigation of reflection signatures (amplitude vs. offset, AVO) of englacial reflectors seems difficult due to the small reflection coefficients, and the small range they cover with changing incoming angle.

For englacial reflections caused by changing COF the variations in the reflection coefficient with offset are very small. The variation of the PP-reflection coefficient for the transition from isotropic to VSM-fabric ($\varphi = 0^\circ$, Fig. 5) from 0° to 60° is only between 0.019 and 0.036. It cannot be expected that the error bars for determining the reflection coefficient of englacial reflections would be smaller than those given for the bed reflection coefficients. Peters et al. (2008) analysed reflection coefficient for the ice bed interface and give error bars $\geq \pm 0.04$. The change in the reflection coefficient with offset for englacial reflections that we calculate is smaller than the given error bars. Thus, it is unlikely that it is possible to derive information about the anisotropic fabric from englacial reflections using AVO analysis. To be able to derive fabric information from AVO analysis the error in determining the reflection coefficient from seismic data needs to be reduced, e.g. better shooting techniques to reduce the signal-to-noise ratio (SNR) in the data or a better understanding of the source amplitude as well as the damping of seismic waves in ice.

4.5 Reflection coefficients for ice–bed interfaces

Of special interest is the determination of the properties of the ice–bed interface from seismic data. It is possible to determine the bed properties below an ice sheet or glacier by analysing the normal incident reflection coefficient (e.g. Smith, 2007) or by AVO analysis (Anandakrishnan, 2003; Peters et al., 2008). Fig. 6 shows reflection coefficients for the transition from isotropic and anisotropic (VSM-fabric) ice to different possible bed properties (Table 2). The properties, P-wave and S-wave velocity and density, for the different bed scenarios and the isotropic ice are taken from Peters et al. (2008). For the anisotropic VSM-fabric the elasticity tensor of Gammon et al. (1983) is used.

Exact solutions are calculated using the equations given by Graebner (1992), with corrections by Ruger (2002). Their equations were used to calculate the exact reflection coefficients for the isotropic ice above the bed (solid lines) and for the anisotropic ice above the bed (dashed lines) shown in Fig. 6. The approximate reflection coefficients for the isotropic ice above the bed (dotted lines) are calculated using equations given in Aki and Richards (2002). The approximate reflection coefficients for the VSM-fabric above the bed (dashed-dotted lines) are calculated using equations given in Ruger (1997).

The differences between the isotropic (solid lines) and anisotropic reflection coefficients (dashed lines) are small (≤ 0.04) for the exact solutions. The approximate calculations fit well to the exact solutions up to a group angle of about 30° , with differences in the same order as isotropic to anisotropic variations. However, differences between exact and approximate reflection coefficients become large for increasing phase angle ($\geq 30^\circ$). Thus, errors introduced by using approximate calculations for the reflection coefficients are larger than the effect of anisotropic ice fabric above the bed.

Peters et al. (2008) analysed the reflection amplitude from a survey near the South Pole. For the reflection coefficients they derive from the seismic data they give error bars ± 0.04 , with increasing error bars for decreasing incoming angles, limited by ± 0.2 . However, the variation observable for reflection coefficients between an isotropic and

Seismic wave propagation in anisotropic ice – Part 1

A. Diez and O. Eisen

[Title Page](#)[Abstract](#)[Introduction](#)[Conclusions](#)[References](#)[Tables](#)[Figures](#)[Back](#)[Close](#)[Full Screen / Esc](#)[Printer-friendly Version](#)[Interactive Discussion](#)

Seismic wave propagation in anisotropic ice – Part 1

A. Diez and O. Eisen

Title Page

Abstract

Introduction

Conclusions

References

Tables

Figures



Back

Close

Full Screen / Esc

Printer-friendly Version

Interactive Discussion



a VSM-fabric overburden are ≤ 0.04 . The VSM-fabric is the strongest anisotropy to be expected in ice. If an anisotropic layer exists above the bed, it influences the reflection coefficient compared to the isotropic ice overburden. However, the difference between the isotropic overburden reflection coefficient and the anisotropic overburden reflection coefficient is within the range of the error bars given by Peters et al. (2008). Thus, the anisotropic fabric will not have an influence on the analysis of the bed properties by means of the AVO method.

5 Conclusions

We presented an approach to derive the elasticity tensor, required for the calculation of seismic wave propagation in anisotropic material, from the COF eigenvalues derived from ice-core measurements. From the elasticity tensors we derived seismic phase and group velocities of P-, SH- and SV-waves for cone, partial girdle and thick girdle structures, i.e. orthorhombic media. We could find good agreement between the velocities derived with our approach and velocities calculated from the equations given by Bennett (1988) for cone fabrics. However, we extend existing theories and algorithms and are now able to investigate the velocity variations in dependency of the incoming angle for different girdle distributions and the reflection coefficients in anisotropic ice as well.

We used the elasticity tensor to derive the reflection signature for englacial fabric changes and investigated the influence of anisotropic fabric on the reflection coefficients for basal reflectors. We found that the reflection coefficients and the variations of the reflection coefficients with increasing offset are weak for the transition between different COF distributions. They are at least an order of magnitude smaller than reflections from the ice–bed interface. Thus, either significant changes in the COF distribution or extremely sensitive measurement techniques are needed to observe englacial seismic reflections. The influence of anisotropic ice fabric compared to the isotropic case for the reflection at the ice–bed interface is so small that it is within the measurement

inaccuracy of currently employed seismic AVO analysis. An important result is that the difference between exact and approximate calculations of reflection coefficients for the ice–bed interface is larger than the influence of an anisotropic ice fabric above the bed. This implies that exact calculations are necessary if the fabric above the bed is in the focus of AVO analysis.

Better results in the calculation of the elasticity tensor could probably be gained by calculation of the opening angles directly from the c-axes vectors. This would avoid our classification into cone, partial girdle and thick girdle fabric. Nevertheless, the approach presented here offers the opportunity to use the readily available COF data from ice cores and go towards an investigation of the seismic wavefield in ice without the limitation to velocities only. The inclusion of further properties influencing the propagation of seismic waves in ice, like density and temperature, will offer the opportunity to model the complete wave field. Hence, we are confident that it will become feasible in the future to derive physical properties of the ice from analyses of the complete observed wave field by full waveform inversions.

Appendix A: From COF eigenvalues to elasticity tensor for seismics

A1 Connection of eigenvalues to opening angles

The following equations give the connection between the eigenvalues λ_1, λ_2 and λ_3 and the two opening angles φ and χ .

For a cone fabric the angle $\varphi = \chi$ is calculated by

$$\varphi = \chi = b_1 \sin(c_1 \lambda_3 + d_1) + b_2 \sin(c_2 \lambda_3 + d_2) + b_3 \sin(c_3 \lambda_3 + d_3) + b_4 \sin(c_4 \lambda_3 + d_4), \quad (\text{A1})$$

with

$$b_1 = 141.9, c_1 = 6.251, d_1 = 2.157,$$

$$b_2 = 139, c_2 = 10.33, d_2 = -1.809,$$

$$b_3 = 90.44, c_3 = 14.68, d_3 = 4.685,$$

$$5 \quad b_4 = 36.61, c_4 = 16.9, d_4 = 12.63.$$

For a thick girdle fabric the angle χ is calculated by

$$\chi = p_1 \lambda_1^7 + p_2 \lambda_1^6 + p_3 \lambda_1^5 + p_4 \lambda_1^4 + p_5 \lambda_1^3 + p_6 \lambda_1^2 + p_7 \lambda_1 + p_8, \quad (\text{A2})$$

$$10 \quad \varphi = 90^\circ, \quad (\text{A3})$$

with

$$p_1 = 2.957 \times 10^7, p_2 = -3.009 \times 10^7, p_3 = 1.233 \times 10^7, p_4 = -2.599 \times 10^6,$$

$$p_5 = 3.023 \times 10^5, p_6 = -1.965 \times 10^4, p_7 = 877.6, p_8 = 2.614.$$

15 For a partial girdle fabric the angle φ is calculated by

$$\varphi = a_1 \sin(b_1 \lambda_3 + c_1) + a_2 \sin(b_2 \lambda_3 + c_2) + a_3 \sin(b_3 \lambda_3 + c_3) + a_4 \sin(b_4 \lambda_3 + c_4), \quad (\text{A4})$$

$$\chi = 0^\circ, \quad (\text{A5})$$

with

$$20 \quad a_1 = 118.7, b_1 = 7.415, c_1 = -3.517,$$

$$a_2 = 97.47, b_2 = 13.68, c_2 = 1.161,$$

$$a_3 = 46.57, b_3 = 18.58, c_3 = 6.935,$$

$$a_4 = 7.455, b_4 = 25.18, c_4 = 11.47.$$

Seismic wave propagation in anisotropic ice – Part 1

A. Diez and O. Eisen

Title Page

Abstract

Introduction

Conclusions

References

Tables

Figures

◀

▶

◀

▶

Back

Close

Full Screen / Esc

Printer-friendly Version

Interactive Discussion



A2 Rotation matrices for elasticity and compliance tensor

Here the rotation matrix for the elasticity tensor and compliance tensor following Sunder and Wu (1994) are given. For the calculation of the elasticity tensor for different fabrics the monocystal elasticity tensor needs to be rotated (Sect. 3.2).

5 The rotation matrix for the elasticity tensor is

$$\mathbf{R}^C = \begin{pmatrix} l_1^2 & m_1^2 & n_1^2 & 2m_1n/l_1 & 2n_1l_1 & 2l_1m_1 \\ l_2^2 & m_2^2 & n_2^2 & 2m_2n/l_2 & 2n_2l_2 & 2l_2m_2 \\ l_3^2 & m_3^2 & n_3^2 & 2m_3n/l_3 & 2n_3l_3 & 2l_3m_3 \\ l_2/l_3 & m_2m_3 & n_2n_3 & m_2n_3 - m_3n_2 & n_2l_3 - n_3l_2 & l_2m_3 - l_3m_2 \\ l_3/l_1 & m_3m_1 & n_3n_1 & m_3n_1 - m_1n_3 & n_3l_1 - n_1l_3 & l_3m_1 - l_1m_3 \\ l_1/l_2 & m_1m_2 & n_1n_2 & m_1n_2 - m_2n_1 & n_1l_2 - n_2l_1 & l_1m_2 - l_2m_1 \end{pmatrix}, \quad (\text{A6})$$

and the compliance tensor

$$\mathbf{R}^S = \begin{pmatrix} l_1^2 & m_1^2 & n_1^2 & m_1n/l_1 & n_1l_1 & l_1m_1 \\ l_2^2 & m_2^2 & n_2^2 & m_2n/l_2 & n_2l_2 & l_2m_2 \\ l_3^2 & m_3^2 & n_3^2 & m_3n/l_3 & n_3l_3 & l_3m_3 \\ 2l_2/l_3 & 2m_2m_3 & 2n_2n_3 & m_2n_3 - m_3n_2 & n_2l_3 - n_3l_2 & l_2m_3 - l_3m_2 \\ 2l_3/l_1 & 2m_3m_1 & 2n_3n_1 & m_3n_1 - m_1n_3 & n_3l_1 - n_1l_3 & l_3m_1 - l_1m_3 \\ 2l_1/l_2 & 2m_1m_2 & 2n_1n_2 & m_1n_2 - m_2n_1 & n_1l_2 - n_2l_1 & l_1m_2 - l_2m_1 \end{pmatrix}, \quad (\text{A7})$$

with the following direction cosines

$$\begin{pmatrix} l_1 & l_2 & l_3 \\ m_1 & m_2 & m_3 \\ n_1 & n_2 & n_3 \end{pmatrix}, \quad (\text{A8})$$

Title Page

Abstract

Introduction

Conclusions

References

Tables

Figures



Back

Close

Full Screen / Esc

Printer-friendly Version

Interactive Discussion



for rotation around the x_1 -axis

$$\begin{pmatrix} 1 & 0 & 0 \\ \cos \phi & -\sin \phi & 0 \\ \sin \phi & \cos \phi & 0 \end{pmatrix}, \quad (\text{A9})$$

for rotation around the x_2 -axis

$$5 \quad \begin{pmatrix} \cos \phi & 0 & -\sin \phi \\ 0 & 1 & 0 \\ \sin \phi & 0 & \cos \phi \end{pmatrix}, \quad (\text{A10})$$

and for rotation around the x_3 -axis

$$\begin{pmatrix} \cos \phi & -\sin \phi & 0 \\ \sin \phi & \cos \phi & 0 \\ 0 & 0 & 1 \end{pmatrix}. \quad (\text{A11})$$

10 **A3 Components of elasticity and compliance tensor for polycrystal**

The components of the polycrystal elasticity tensor as derived from Eq. (12) with c-axes distribution around the x_1 -axis, i.e. within the $[x_2, x_3]$ -plane are calculated by:

$$\begin{aligned} C_{11}^p &= C_{11}^m, \\ C_{22}^p &= \frac{1}{2\phi_0} [b_1 C_{22}^m + b_2 C_{33}^m + 2b_3 (C_{23}^m + 2C_{44}^m)], \\ 15 \quad C_{33}^p &= \frac{1}{2\phi_0} [b_1 C_{33}^m + b_2 C_{22}^m + 2b_3 (C_{23}^m + 2C_{44}^m)], \\ C_{44}^p &= \frac{1}{2\phi_0} [(b_1 + b_2) C_{44}^m + b_3 (C_{22}^m - 2C_{23}^m + C_{33}^m - 2C_{44}^m)], \\ C_{55}^p &= \frac{1}{2\phi_0} [C_{55}^m (\phi_0 + \alpha) + C_{66}^m (\phi_0 - \alpha)], \end{aligned}$$

Seismic wave propagation in anisotropic ice – Part 1

A. Diez and O. Eisen

[Title Page](#)
[Abstract](#)
[Introduction](#)
[Conclusions](#)
[References](#)
[Tables](#)
[Figures](#)
[Back](#)
[Close](#)
[Full Screen / Esc](#)
[Printer-friendly Version](#)
[Interactive Discussion](#)


$$\begin{aligned}
 C_{66}^p &= \frac{1}{2\phi_0} [C_{66}^m(\phi_0 + \alpha) + C_{55}^m(\phi_0 - \alpha)], \\
 C_{12}^p &= \frac{1}{2\phi_0} [C_{12}^m(\phi_0 + \alpha) + C_{13}^m(\phi_0 - \alpha)], \\
 C_{13}^p &= \frac{1}{2\phi_0} [C_{13}^m(\phi_0 + \alpha) + C_{12}^m(\phi_0 - \alpha)], \\
 C_{23}^p &= \frac{1}{2\phi_0} [(b_1 + b_2)C_{23}^m + b_3(C_{22}^m - 4C_{44}^m + C_{33}^m)].
 \end{aligned} \tag{A12}$$

The components of the polycrystal compliance tensor as derived from Eq. (13) with c-axes distribution around the x_1 -axis, i.e. within the $[x_2, x_3]$ -plane are calculated by:

$$\begin{aligned}
 S_{11}^p &= S_{11}^m, \\
 S_{22}^p &= \frac{1}{2\phi_0} [b_1 S_{22}^m + b_2 S_{33}^m + b_3(2S_{23}^m + S_{44}^m)], \\
 S_{33}^p &= \frac{1}{2\phi_0} [b_1 S_{33}^m + b_2 S_{22}^m + b_3(2S_{23}^m + S_{44}^m)], \\
 S_{44}^p &= \frac{1}{2\phi_0} \left[(b_1 + b_2)S_{44}^m + 4b_3(S_{22}^m - 2S_{23}^m + S_{33}^m - \frac{1}{2}S_{44}^m) \right], \\
 S_{55}^p &= \frac{1}{2\phi_0} [S_{55}^m(\phi_0 + \alpha) + S_{66}^m(\phi_0 - \alpha)], \\
 S_{66}^p &= \frac{1}{2\phi_0} [S_{66}^m(\phi_0 + \alpha) + S_{55}^m(\phi_0 - \alpha)], \\
 S_{12}^p &= \frac{1}{2\phi_0} [S_{12}^m(\phi_0 + \alpha) + S_{13}^m(\phi_0 - \alpha)], \\
 S_{13}^p &= \frac{1}{2\phi_0} [S_{13}^m(\phi_0 + \alpha) + S_{12}^m(\phi_0 - \alpha)],
 \end{aligned}$$

$$S_{23}^p = \frac{1}{2\phi_0} [(b_1 + b_2)S_{23}^m + b_3(S_{22}^m - S_{44}^m + S_{33}^m)]. \quad (\text{A13})$$

These variables apply for the equations for the calculation of the elasticity and compliance tensor of the polycrystal:

$$\begin{aligned} b_1 &= \frac{3}{4}\phi_0 + \alpha + \beta, \\ b_2 &= \frac{3}{4}\phi_0 - \alpha + \beta, \\ b_3 &= \frac{1}{4}\phi_0 - \beta, \\ \alpha &= \frac{1}{2}\sin 2\phi_0, \\ \beta &= \frac{1}{16}\sin 4\phi_0. \end{aligned} \quad (\text{A14})$$

Appendix B: Equations for calculation of velocities and reflection coefficients

B1 Velocities in anisotropic media

To be able to calculate velocities for partial girdle fabric the calculation of phase velocity for orthorhombic media derived by Daley and Krebs (2004) is used. They rearrange linearised equations to obtain the velocity from an ellipsoidal part with an ellipsoidal correction term:

$$v_p(\mathbf{n}) = \sqrt{1/\rho(C_{11}n_1^2 + C_{22}n_2^2 + C_{33}n_3^2 + 2B_{12}n_1^2n_2^2 + 2B_{13}n_1^2n_3^2 + 2B_{23}n_2^2n_3^2)}, \quad (\text{B1})$$

$$v_{sv}(\mathbf{n}) = \sqrt{1/\rho(C_{44}\sin^2\psi + C_{55}\cos^2\psi + 2B_{12}n_1^2n_3^2\sin^2\psi - 2B_{13}n_2^2n_3^2 - 2B_{23}n_1^2n_3^2)}, \quad (\text{B2})$$

$$v_{\text{sh}}(\mathbf{n}) = \sqrt{1/\rho(C_{44}n_3^2 \cos^2 \psi + C_{55}n_3^2 \sin^2 \psi + C_{66} \sin^2 \vartheta - 2B_{12}n_1^2 \sin^2 \psi)}, \quad (\text{B3})$$

with

$$B_{12} = (C_{13} + 2C_{66}) - (C_{11} + C_{22})/2, \quad (\text{B4})$$

$$B_{13} = (C_{12} + 2C_{55}) - (C_{11} + C_{33})/2, \quad (\text{B5})$$

$$B_{23} = (C_{23} + 2C_{44}) - (C_{22} + C_{33})/2, \quad (\text{B6})$$

and the unit phase normal vector

$$\mathbf{n} = (n_1, n_2, n_3) = (\sin \vartheta \cos \psi, \sin \vartheta \sin \psi, \cos \vartheta). \quad (\text{B7})$$

with the phase angle ϑ and the azimuth ψ , here the azimuth for the orientation of a girdle fabric (Fig. 1).

The components of the group velocity vector are given by (Tsvankin, 2001)

$$v_{g,x_1} = v \sin \vartheta + \left. \frac{\partial v_{\text{ph}}}{\partial \vartheta} \right|_{\psi=\text{const}} \cos \vartheta, \quad (\text{B8})$$

$$v_{g,x_2} = \frac{1}{\sin \vartheta} \left. \frac{\partial v_{\text{ph}}}{\partial \psi} \right|_{\vartheta=\text{const}}, \quad (\text{B9})$$

$$v_{g,x_3} = v_{\text{ph}} \cos \vartheta + \left. \frac{\partial v_{\text{ph}}}{\partial \vartheta} \right|_{\psi=\text{const}} \sin \vartheta. \quad (\text{B10})$$

Within the symmetry planes the group velocity can be calculated using v_{g,x_1} and v_{g,x_3} only (Eq. 14).

Outside the symmetry planes of the HTI media the component v_{g,x_2} can not be neglected as the derivation $\frac{\partial v}{\partial \psi}$ is no longer zero. In this case v_g is the norm of the group

velocity vector \mathbf{v}_g considering all three components v_{g,x_1} , v_{g,x_2} and v_{g,x_3} . Here, a second group angle (next to the one in the plane Eq. 15) exists for the direction outside the plane with

$$\tan \theta_{\text{out}} = \frac{v_{g,x_2}}{\sqrt{v_{g,x_1}^2 + v_{g,x_3}^2}}. \quad (\text{B11})$$

B2 Reflection coefficients (Zillmer)

The reflection coefficients as derived by Zillmer et al. (1997, 1998a) are given by

$$R_{\text{pp}} = \frac{1}{4} \left(\frac{\Delta C_{33}}{C_{44}^{(0)} + 2C_{12}^{(0)}} + \frac{\Delta \rho}{\rho^{(0)}} \right) - \frac{1}{4} \frac{\Delta \rho}{\rho^{(0)}} \tan^2(\vartheta) + \frac{1}{4} \frac{2\Delta C_{13} - C_{33} - 4\Delta C_{55}}{C_{44}^{(0)} + 2C_{12}^{(0)}} \sin^2 \vartheta + \frac{1}{4} \frac{\Delta C_{11}}{C_{44}^{(0)} + 2C_{12}^{(0)}} \sin^2 \vartheta \tan^2 \vartheta, \quad (\text{B12})$$

$$R_{\text{svsv}} = -\frac{1}{4} \left(\frac{\Delta C_{55}}{C_{12}^{(0)}} + \frac{\Delta \rho}{\rho^{(0)}} \right) - \frac{1}{4} \frac{\Delta \rho}{\rho^{(0)}} \tan^2(\vartheta) + \frac{1}{4} \frac{\Delta C_{11} - 2\Delta C_{13} + C_{33} - 3\Delta C_{55}}{C_{12}^{(0)}} \sin^2 \vartheta - \frac{1}{4} \frac{\Delta C_{55}}{C_{12}^{(0)}} \sin^2 \vartheta \tan^2 \vartheta, \quad (\text{B13})$$

$$R_{\text{shsh}} = -\frac{1}{4} \left(\frac{\Delta C_{44}}{C_{12}^{(0)}} + \frac{\Delta \rho}{\rho^{(0)}} \right) + \frac{1}{4} \left(\frac{\Delta C_{66}}{C_{12}^{(0)}} + \frac{\Delta \rho}{\rho^{(0)}} \right) \tan^2 \vartheta, \quad (\text{B14})$$

where Δ denotes the difference between the upper layer 1 and the lower layer 2, for example $\Delta C_{33} = C_{33}^{(2)} - C_{33}^{(1)}$. The superscript (0) gives the isotropic reference values. When reflection coefficients are calculated for different anisotropic ice fabrics, the density is constant, i.e. the $\Delta\rho$ -terms can be neglected ($\rho^{(2)} - \rho^{(1)} = 0$).

Acknowledgements. We thank T. Bohlen and his group of the Karlsruhe Institute of Technology for their support and numerous hints during this study. Financial support for this study was provided to O.E. by the Deutsche Forschungsgemeinschaft (DFG) “Emmy Noether”-program grant EI 672/5-1.

The service charges for this open access publication have been covered by a Research Centre of the Helmholtz Association.

References

- Aki, K. and Richards, P. G.: Quantitative Seismology, University Science Books Sausalito, California, 2002. 4357, 4369, 4372, 4395
- Anandakrishnan, S.: Dilatant till layer near the onset of streaming flow of Ice StreamC, West Antarctica, determined by AVO (amplitude vs. offset) analysis, *Ann. Glaciol.*, 36, 283–286, 2003. 4372
- Ashby, M. F. and Duval, P.: The creep of polycrystalline ice, *Cold Reg. Sci. Technol.*, 11, 285–300, 1985. 4351
- Bass, R., Rossberg, D., and Ziegler, G.: Die elastischen Konstanten des Eises, *Z. Phys.*, 149, 199–203, 1957. 4365
- Bell, R. E., Ferraccioli, F., Creyts, T. T., Braaten, D., Corr, H., Das, I., Damaske, D., Frearson, N., Jordan, T., Rose, K., Studinger, M., and Wolovick, M.: Widespread persistent thickening of the East Antarctic Ice Sheet by freezing from the base, *Science*, 331, 1592–1595, doi:10.1126/science.1200109, 2011. 4351
- Bennett, H. F.: An investigation into velocity anisotropy through measurements of ultrasonic wave velocities in snow and ice cores from Greenland and Antarctica, Ph. D. thesis, University of Wisconsin-Madison, Ann Arbor, MI, UMI, 1988. 4353, 4365, 4366, 4368, 4369, 4373, 4393
- Bentley, C. R.: Seismic c wave velocities in anisotropic ice: a comparison of measured and calculated values in and around the deep drill hole at Byrd Station, Antarctica, *J. Geophys. Res.*, 77, 4406–4420, 1972. 4353

Seismic wave propagation in anisotropic ice – Part 1

A. Diez and O. Eisen

Title Page

Abstract

Introduction

Conclusions

References

Tables

Figures

◀

▶

◀

▶

Back

Close

Full Screen / Esc

Printer-friendly Version

Interactive Discussion



Seismic wave propagation in anisotropic ice – Part 1

A. Diez and O. Eisen

Title Page

Abstract

Introduction

Conclusions

References

Tables

Figures

◀

▶

◀

▶

Back

Close

Full Screen / Esc

Printer-friendly Version

Interactive Discussion



Blankenship, D. D. and Bentley, C. R.: The crystalline fabric of polar ice sheets inferred from seismic anisotropy, in: The Physical Basis of Ice Sheet Modelling (Proceedings of the Vancouver Symposium, August 1987, IAHS Publ., 54–57, 1987. 4353

Bower, A. F.: Applied Mechanics of Solids, CRC Press, Boca Raton, FL., 2010. 4362

5 Brockamp, B. and Querfurth, H.: Untersuchungen über die Elastizitätskonstanten von See- und Kunsteis, Polarforschung, 34, 253–262, 1964. 4365

Cuffey, K. M. and Paterson, W. S. B.: The Physics of Glaciers, Elsevier, 4th edn. Butterworth-Heinemann, Oxford, 2010. 4350, 4351, 4355

10 Daley, P. and Heron, F.: Reflection and transmission coefficients for transversely isotropic media, Bulletin of the Seismological Society of America (BSSA), 67, 661–675, 1977. 4366, 4369

Daley, P. F. and Krebes, E. S.: Alternative linearized expressions for qP , $qS1$ and $qS2$ phase velocities in a weakly anisotropic orthorhombic medium, CREWES Research Reports, Consortium for Research in Elastic Wave Exploration Seismology, <http://www.crewes.org/ForOurSponsors/ResearchReports/>, 16, 1–19, 2004. 4366, 4367, 4368, 4379, 4393

15 Dantl, G.: Die elastischen Moduln von Eis-Einkristallen, Phys. Kondens. Mater., 7, 390–397, 1968. 4365

Diez, A.: Effects of Cold Glacier Ice Crystal Anisotropy on Seismic Data, Ph. D. thesis, Karlsruhe Institute of Technology, Karlsruhe, Germany, 2013. 4368

20 Diez, A., Eisen, O., Hofstede, C., Bohleber, P., and Polom, U.: Joint interpretation of explosive and vibroseismic surveys on cold firn for the investigation of ice properties, Ann. Glaciol., 54, 201–210, 2013. 4371

Diez, A., Eisen, O., Weikusat, I., Hofstede, T. B. C., Lambrecht, A., Mayer, C., Miller, H., and Steinahge, D.: Seismic wave propagation in anisotropic ice – Part 2: Inference of physical properties from geophysical data, The Cryosphere, in press, 2014. 4354, 4359, 4365

25 Drews, R., Eisen, O., Weikusat, I., Kipfstuhl, S., Lambrecht, A., Steinhage, D., Wilhelms, F., and Miller, H.: Layer disturbances and the radio-echo free zone in ice sheets, The Cryosphere, 3, 195–203, doi:10.5194/tc-3-195-2009, 2009. 4351

30 Drews, R., Martin, C., Steinhage, D., and Eisen, O.: Characterizing the glaciological conditions at Halvfarryggen ice dome, Dronning Maud Land, Antarctica, J. Glaciol., 59, 9–20, 2013. 4351

Seismic wave propagation in anisotropic ice – Part 1

A. Diez and O. Eisen

[Title Page](#)[Abstract](#)[Introduction](#)[Conclusions](#)[References](#)[Tables](#)[Figures](#)[Back](#)[Close](#)[Full Screen / Esc](#)[Printer-friendly Version](#)[Interactive Discussion](#)

Eisen, O., Hamann, I., Kipfstuhl, S., Steinhage, D., and Wilhelms, F.: Direct evidence for continuous radar reflector originating from changes in crystal-orientation fabric, *The Cryosphere*, 1, 1–10, doi:10.5194/tc-1-1-2007, 2007. 4352

Elvin, A. A.: Number of grains required to homogenize elastic properties of polycrystalline ice, *Mech. Mater.*, 22, 51–64, 1996. 4365

Faria, S. H., Weikusat, I., and Azuma, N.: The microstructure of polar ice. Part II: State of the art, *J. Struct. Geol.*, 61, 21–49, doi:10.1016/j.jsg.2013.11.003, 2014a. 4355

Faria, S. H., Weikusat, I., and Azuma, N.: The microstructure of polar ice. Part I: Highlights from ice core research, *J. Struct. Geol.*, 61, 2–20, doi:10.1016/j.jsg.2013.09.010, 2014b. 4352

Fischer, H., Severinghaus, J., Brook, E., Wolff, E., Albert, M., Alemany, O., Arthern, R., Bentley, C., Blankenship, D., Chappellaz, J., Creyts, T., Dahl-Jensen, D., Dinn, M., Frezzotti, M., Fujita, S., Gallee, H., Hindmarsh, R., Hudspeth, D., Jugie, G., Kawamura, K., Lipenkov, V., Miller, H., Mulvaney, R., Parrenin, F., Pattyn, F., Ritz, C., Schwander, J., Steinhage, D., van Ommen, T., and Wilhelms, F.: Where to find 1.5 million yr old ice for the IPICS “Oldest-Ice” ice core, *Clim. Past*, 9, 2489–2505, doi:10.5194/cp-9-2489-2013, 2013. 4352

Fujita, S., Maeno, H., and Matsuoka, K.: Radio wave depolarization and scattering within ice sheets: a matrix-based model to link radar and ice-core measurements and its application, *J. Glaciol.*, 52, 407–424, 2006. 4352

Gammon, P. H., Kieffe, H., Clouter, M. J., and Denner, W. W.: Elastic constant of artificial and natural ice samples by brillouin spectroscopy, *J. Glaciol.*, 29, 433–460, 1983. 4359, 4365, 4368, 4369, 4372, 4395

Graebner, M.: Plane wave reflection and transmission coefficients for a transversely isotropic solid, *Geophysics*, 57, 1512–1519, doi:10.1190/1.1443219, 1992. 4366, 4370, 4372, 4395

Green, R. E. and Mackinnen, L.: Determination of the Elastic Constants of ice single crystal by ultrasonic pulse method, *J. Acoust. Soc. Am.*, 28, p. 1292, 1956. 4365

Gusmeroli, A., Pettit, E. C., Kennedy, J. H., and Ritz, C.: The crystal fabric of ice from full wave-form borehole sonic logging, *J. Geophys. Res.*, 117, F03021, doi:10.1029/2012JF002343, 2012. 4353

Hill, R.: The elastic behaviour of a crystalline aggregate, *P. Phys. Soc. Lond. A*, 65, 349–354, 1952. 4362

Hofstede, C., Eisen, O., Diez, A., Jansen, D., Kristoffersen, Y., Lambrecht, A., and Mayer, C.: Investigating englacial reflections with vibro- and explosive-seismic surveys at Halvfarryggen ice dome, Antarctica, *Ann. Glaciol.*, 54, 189–200, 2013. 4353, 4371

**Seismic wave
propagation in
anisotropic ice –
Part 1**

A. Diez and O. Eisen

[Title Page](#)[Abstract](#)[Introduction](#)[Conclusions](#)[References](#)[Tables](#)[Figures](#)[◀](#)[▶](#)[◀](#)[▶](#)[Back](#)[Close](#)[Full Screen / Esc](#)[Printer-friendly Version](#)[Interactive Discussion](#)

Horgan, H. J., Anandakrishnan, S., Alley, R. B., Peters, L. E., Tsoflias, G. P., Voigt, D. E., and Winberry, J. P.: Complex fabric development revealed by englacial seismic reflectivity: Jakobshavn Isbræ, Greenland, *Geophys. Res. Lett.*, 35, L10501, doi:10.1029/2008GL033712, 2008. 4353, 4371

5 Horgan, H. J., Anandakrishnan, S., Alley, R. B., Burkett, P. G., and Peters, L. E.: Englacial seismic reflectivity: imaging crystal-orientation fabric in West Antarctica, *J. Glaciol.*, 57, 639–650, 2011. 4353, 4371

Jona, F. and Scherrer, P.: Die elastischen Konstanten von Eis-Einkristallen, *Helv. Phys. Acta*, 25, 35–54, 1952. 4365

10 Keith, C. M. and Crampin, S.: Seismic body waves in anisotropic media: reflection and refraction at a plane interface, *Geophys. J. Roy. Astr. S.*, 49, 181–208, 1977. 4369, 4370

Kohnen, H.: The temperature dependence of seismic waves in ice, *J. Glaciol.*, 13, 144–147, 1974. 4368

15 Martín, C., Gudmundsson, G. H., Pritchard, H. D., and Gagliardini, O.: On the effects of anisotropic rheology on ice flow, internal structure, and the age–depth relationship at ice divides, *J. Geophys. Res.*, 114, 1–18, 2009a. 4351

Martín, C., Hindmarsh, R. C. A., and Navarro, F. J.: On the effects of divide migration, along-ridge flow, and basal sliding on isochrones near an ice divide, *J. Geophys. Res.-Earth*, 114, F02006, doi:10.1029/2008JF001025, 2009b. 4351

20 Matsuoka, K., Furukawa, T., Fujita, S., Maeno, H., Urantsuka, S., Naruse, R., and Watanabe, O.: Crystal orientation fabrics within the Antarctic ice sheet revealed by a multipolarization plane and dual-frequency radar survey, *J. Geophys. Res.*, 108, 2499, doi:10.1029/2003JB002425, 2003 4352

25 Matsuoka, K., Wilen, L., Huerly, S. P., and Raymond, C. F.: Effects of birefringence within ice sheets on obliquely propagating radio waves, *IEEE T. Geosci. Remote*, 47, 1429–1443, 2009. 4352

Nanthikesan, S. and Sunder, S. S.: Anisotropic elasticity of polycrystalline ice Ih, *Cold Reg. Sci. Technol.*, 22, 149–169, 1994. 4361, 4364

30 NEEM community members: Eemian interglacial reconstructed from a Greenland folded ice core, *Nature*, 493, 489–494, doi:10.1038/nature11789, 2013. 4351

Penny, A. H. A.: A theoretical determination of the elastic constants of ice, *Math. Proc. Cambridge*, 44, 423–439, 1948. 4365

Seismic wave propagation in anisotropic ice – Part 1

A. Diez and O. Eisen

Title Page

Abstract

Introduction

Conclusions

References

Tables

Figures

◀

▶

◀

▶

Back

Close

Full Screen / Esc

Printer-friendly Version

Interactive Discussion



Peternell, M., Hasalova, P., Wilson, C. J. L., Piazzolo, S., and Schulmann, K.: Evaluating quartz crystallographic preferred orientations and the role of deformation partitioning using EBSD and fabric analyser techniques, *J. Struct. Geol.*, 32, 803–817, 2010. 4355

Peters, L. E., Anandakrishnan, S., Holland, C. W., Horgan, H. J., Blankenship, D. D., and Voigt, D. E.: Seismic detection of a subglacial lake near the South Pole, Antarctica, *Geophys. Res. Lett.*, 35, L23501, doi:10.1029/2008GL035704, 2008. 4371, 4372, 4373, 4389, 4395

Pettit, E. C., Thorsteinsson, T., Jacobson, H. P., and Waddington, E. D.: The role of crystal fabric in flow near an ice divide, *J. Glaciol.*, 53, 277–288, doi:10.3189/172756507782202766, 2007. 4351

Polom, U., Hofstede, C., Diez, A., and Eisen, O.: First glacier-vibro seismic experiment-results from the cold firn of Colle Gniefetti, Near Surf. Geophys., 12, 493–504, doi:10.3997/1873-0604.2013059, 2014. 4371

Raymond, C. F.: Deformation in the vicinity of ice divides, *J. Glaciol.*, 29, 357–373, 1983. 4351

Reuss, A.: Berechnung der Fließsgrenzen von Mischkristallen auf Grund der Platizitätsbedingung für Einkristalle, *Zamm-Z. Angew. Math. Me.*, 9, 49–58, 1929. 4361, 4362, 4364

Rommel, B. E. and Tsvankin, I.: Analytic description of P-wave ray direction and polarization in orthorhombic media, in: *Anisotropy 2000: Fractures, Converted Waves, and Case Studies*, edited by: Ilkelle, L. T., Society of Exploration Geophysicists, Proceedings of the 9th International Workshop on Seismic Anisotropy (9IWSA), Soc. Expl. Geophys., 1–19, 2000. 4367

Rüger, A.: P-wave reflection coefficient for transversely isotropic models with vertical and horizontal axis of symmetry, *Geophysics*, 62, 713–722, 1997. 4366, 4370, 4372, 4395

Rüger, A.: Reflection coefficients and azimuthal AVO analysis in anisotropic media, *Soc. Explor. Geophys.*, 10, 202 pp., doi:10.1190/1.9781560801764, 2002. 4369, 4372, 4395

Smith, A. M.: Subglacial bed properties from normal-incidence seismic reflection data, *J. Environ. Eng. Geoph.*, 12, 3–13, 2007. 4372

Sunder, S. S. and Wu, M. S.: Crack nucleation due to elastic anisotropy in polycrystalline ice, *Cold Reg. Sci. Technol.*, 18, 29–47, 1994. 4376

Thomsen, L.: Weak anisotropic reflections, vol. 8 of *Offset-Dependent Reflectivity – Theory and Practice of AVO Analyses*, Investigations in Geophysics Series, Society of Exploration Geophysicists, USA, 1993. 4369, 4370

Seismic wave propagation in anisotropic ice – Part 1

A. Diez and O. Eisen

Title Page

Abstract

Introduction

Conclusions

References

Tables

Figures

◀

▶

◀

▶

Back

Close

Full Screen / Esc

Printer-friendly Version

Interactive Discussion



Tsvankin, I.: Seismic Signatures and Analysis of Reflection Data in Anisotropic Media, vol. 29 of Handbook of Geophysical Exploration, Seismic Expolration, Pergamon, Amsterdam, the Netherlands, 2001. 4358, 4367, 4380

Voigt, W.: Lehrbuch der Kristallphysik: (mit Ausschluss der Kristalloptik), Bibliotheca Mathematica Teubneriana, 12, Johnson, New York, 1910. 4358, 4361, 4362, 4364, 4365

Wallbrecher, E.: Tektonische und Gefügeanalytische Arbeitsweisen, Ferdinand Enke Verlag, Stuttgart, Germany, 1986. 4355, 4356, 4360, 4361

Wilson, C. J. L., Russell-Head, D. S., and Sim, H. M.: The application of an automated fabric analyzer system to the textural evolution of folded ice layers in shear zones, Ann. Glaciol., 37, 7–17, 2003. 4355

Woodcock, N. H.: Specification of fabric shapes using an eigenvalue method, Geol. Soc. Am. Bull., 88, 1231–1236, 1977. 4352, 4360

Zillmer, M., Gajewski, D., and Kashtan, B. M.: Reflection coefficients for weak anisotropic media, Geophys. J. Int., 129, 389–398, 1997. 4369, 4381

Zillmer, M., Gajewski, D., and Kashtan, B. M.: Anisotropic reflection coefficients for a weak-contrast interface, Geophys. J. Int., 132, 159–166, 1998a. 4369, 4370, 4381

Zillmer, M., Gajewski, D., and Kashtan, B. M.: Anisotropic reflection coefficients for a weak-contrast interface, Geophys. J. Int., 132, 159–166, 1998b. 4366

Seismic wave propagation in anisotropic ice – Part 1

A. Diez and O. Eisen

Table 1. Steps for calculation of elasticity tensor (Eq. 13) or compliance tensor (Eq. 13) for different fabrics (Fig. 1).

	step	rotation axis	angle
cone	1	x_1	$\varphi = \chi$
	2	x_3	90°
partial girdle	1	x_1	φ
thick girdle	1	x_1	90°
	2	x_2	χ

Title Page

Abstract

Introduction

Conclusions

References

Tables

Figures



Back

Close

Full Screen / Esc

Printer-friendly Version

Interactive Discussion



Seismic wave propagation in anisotropic ice – Part 1

A. Diez and O. Eisen

Title Page

Abstract

Introduction

Conclusions

References

Tables

Figures

◀

▶

◀

▶

Back

Close

Full Screen / Esc

Printer-friendly Version

Interactive Discussion



Table 2. P- and S-wave velocity as well as density for different bed scenarios and isotropic ice as given in Peters et al. (2008). These values are used for the calculation of reflection coefficients given in Fig. 6.

material	v_p in m s^{-1}	v_s in m s^{-1}	ρ in kg cm^{-3}
ice	3810	1860	920
basement	5200	2800	2700
lithified sediment	3750	2450	2450
dilatant sediment	1700	200	1800
water	1498	0	1000

Seismic wave propagation in anisotropic ice – Part 1

A. Diez and O. Eisen

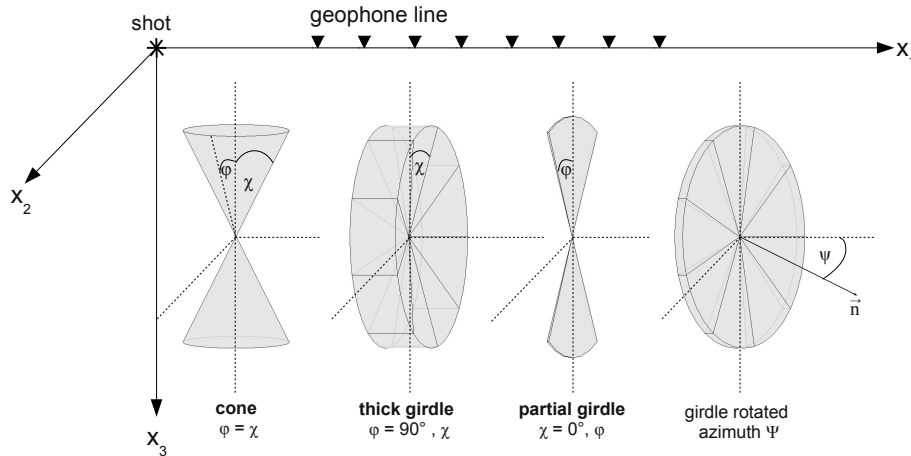


Figure 1. Enveloping of different COF distributions used in the following analysis of seismic data within the used coordinate system. It is distinguished between cone fabric, thick and partial girdle fabric. The cone fabric, seismically a vertical transversely isotropic (VTI) medium, includes the two extreme forms of single vertical maximum and isotropic state. The two girdle fabrics are within the $[x_2, x_3]$ -plane, a horizontal transversely isotropic (HTI) medium and can be turned around the azimuth ψ .

Title Page

Abstract

Introduction

Conclusions

References

Tables

Figures

◀

▶

◀

▶

Back

Close

Full Screen / Esc

Printer-friendly Version

Interactive Discussion



Seismic wave propagation in anisotropic ice – Part 1

A. Diez and O. Eisen

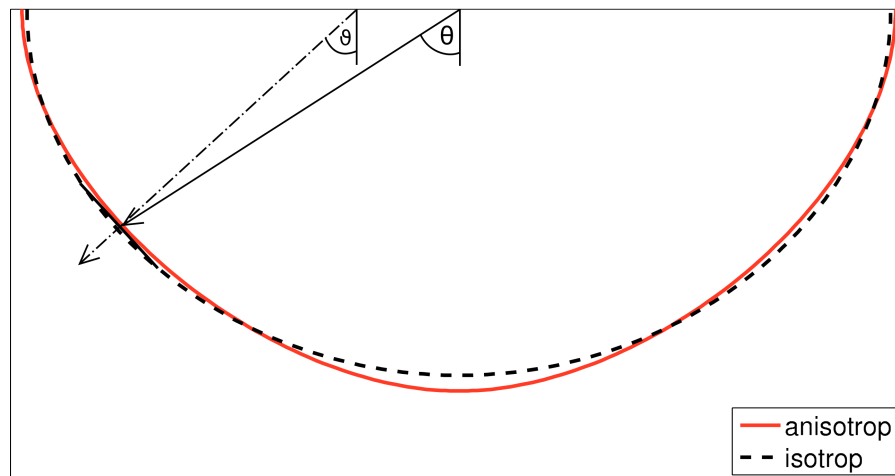


Figure 2. Wavefront of a P-wave travelling in isotropic ice fabric (dashed line) and in an vertical single maximum (VSM) fabric (red line), thus, a vertical transversely isotropic (VTI) media. The solid arrow shows the group velocity with group angle θ , the dashed arrow the phase velocity with phase angle ϑ .

Title Page

Abstract

Introduction

Conclusions

References

Tables

Figures

◀

▶

◀

▶

Back

Close

Full Screen / Esc

Printer-friendly Version

Interactive Discussion



Seismic wave propagation in anisotropic ice – Part 1

A. Diez and O. Eisen

Title Page

Abstract

Introduction

Conclusions

References

Tables

Figures

◀

▶

◀

▶

Back

Close

Full Screen / Esc

Printer-friendly Version

Interactive Discussion

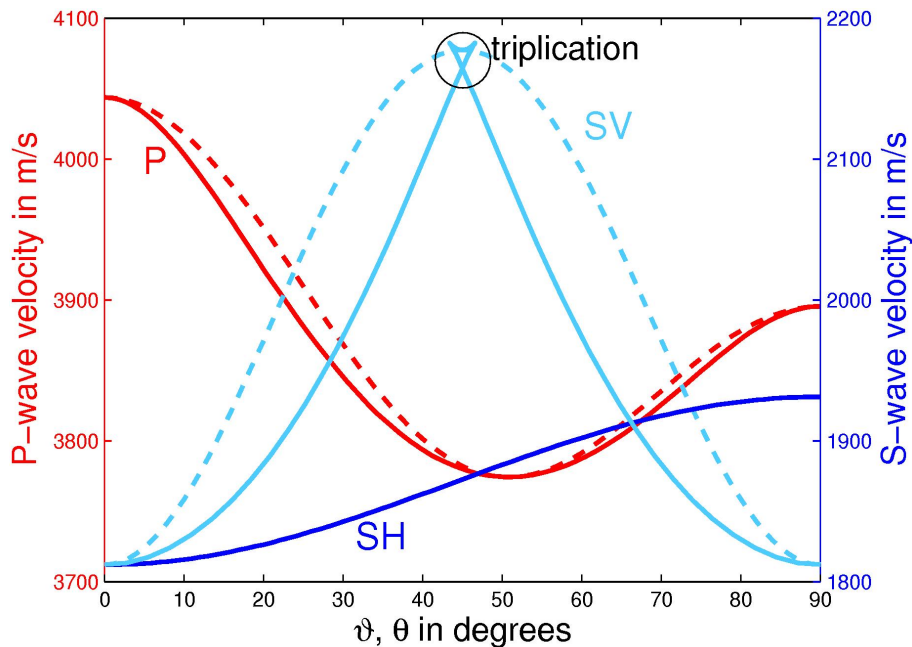


Figure 3. Phase (dashed lines) and group velocities (solid lines) over the corresponding phase ϑ and group angle θ for P- (red curves), SH- (blue curves) and SV-waves (light blue curves) of a VSM-fabric. The SV-wave group velocity shows a triplication. For group angles θ between 43° and 46° three different velocities are given for each angle.

Seismic wave propagation in anisotropic ice – Part 1

A. Diez and O. Eisen

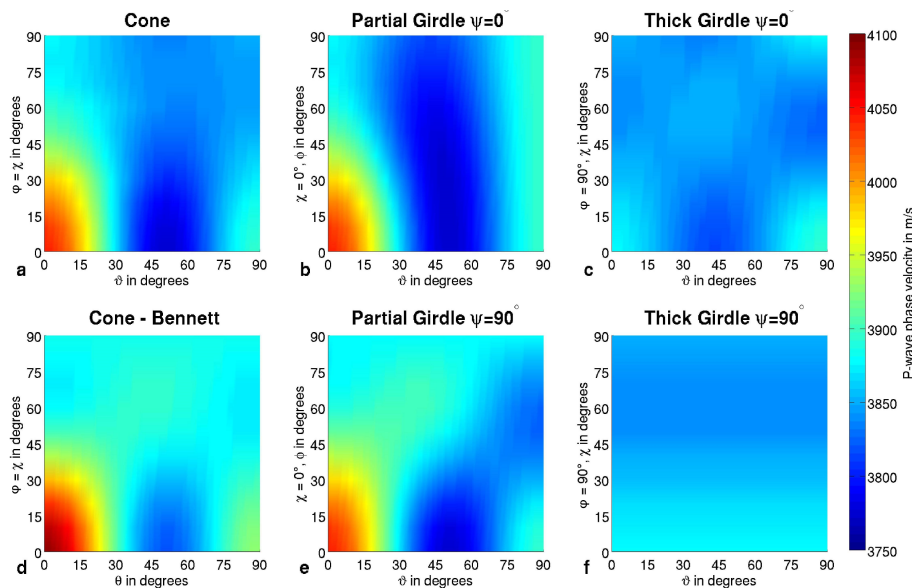


Figure 4. P-wave phase velocities over phase angle ϑ for different fabrics. P-wave velocity for **(a)** different cone opening angles ($\varphi = \chi$), **(b)** partial girdle fabric ($\chi = 0^\circ$) and **(c)** thick girdle fabric ($\varphi = 90^\circ$) within the $[x_2, x_3]$ -plane, **(e)** partial girdle fabric ($\chi = 0^\circ$) and **(f)** thick girdle fabric ($\varphi = 90^\circ$) within the $[x_1, x_3]$ -plane calculated with Eq. (B1) given by Daley and Krebs (2004). **(d)** shows the P-wave velocity for different cone opening angles ($\varphi = \chi$) calculated with the equation given by Bennett (1988).

Title Page

Abstract

Introduction

Conclusions

References

Tables

Figures

◀

▶

◀

▶

Back

Close

Full Screen / Esc

Printer-friendly Version

Interactive Discussion



Seismic wave propagation in anisotropic ice – Part 1

A. Diez and O. Eisen

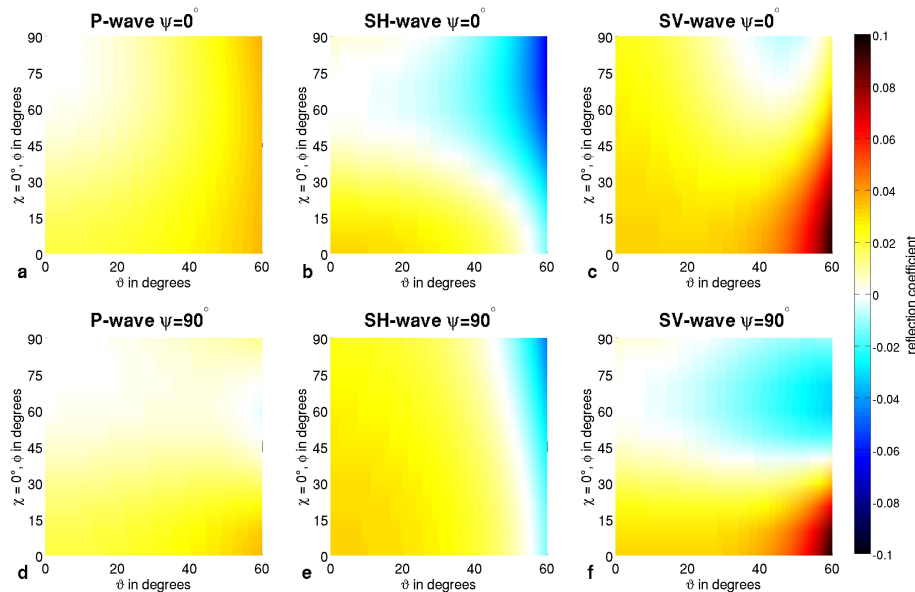


Figure 5. Reflection coefficients for the boundary between an isotropic (upper) layer and a partial girdle fabric (lower) layer with different opening angles φ ($\chi = 0^\circ$) of the girdle. The reflection coefficients are calculated with equations given in Sect. 4.3 for different incoming phase angles ϑ . The subfigures (a), (b) and (c) show the reflection coefficients for a girdle orientation (lower layer) perpendicular to the travelpath of the wave (HTI media) for PP-, SHSH- and SVSV-reflection, respectively. The subfigures (d), (e) and (f) show the reflection coefficients for a girdle orientation parallel to the travelpath of the wave (azimuth $\psi = 90^\circ$) for PP-, SHSH- and SVSV-reflection, respectively.

Seismic wave propagation in anisotropic ice – Part 1

A. Diez and O. Eisen

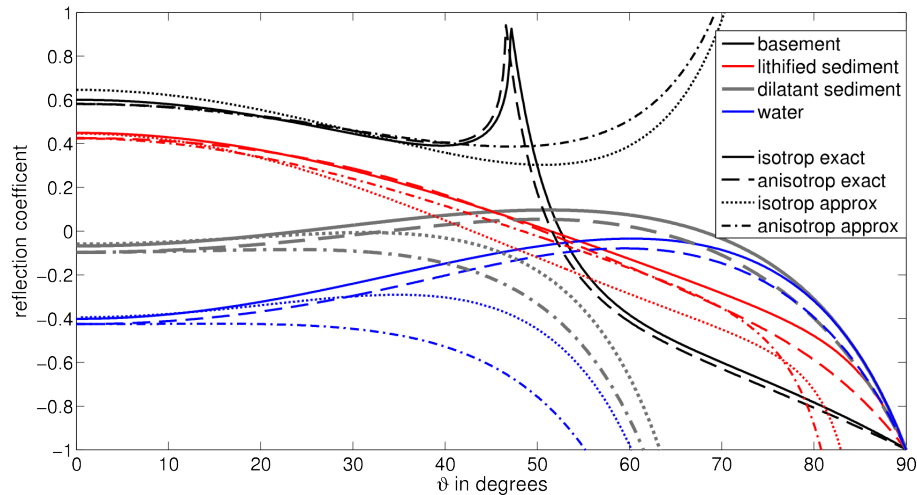


Figure 6. Reflection coefficients for ice-bed interface with different bed properties as a function of phase angle of incidence ϑ : basement (black), lithified sediments (red), dilatant sediments (gray) and water (blue). The solid and dotted lines are the reflection coefficients for an isotropic ice overburden, the dashed and dashed-dotted lines for the anisotropic (VSM) overburden. The solid and dashed lines are the reflection coefficients calculated with exact equations for VTI media given by Graebner (1992) and Rüger (2002). The dotted and dashed-dotted lines are approximate calculations following the approach by Aki and Richards (2002) for the isotropic and that of Rüger (1997) for the anisotropic case, respectively. Bed property values for bed and isotropic ice are taken from Peters et al. (2008), for the anisotropic ice the elasticity tensor given by Gammon et al. (1983) is used.

[Title Page](#)
[Abstract](#)
[Introduction](#)
[Conclusions](#)
[References](#)
[Tables](#)
[Figures](#)
[◀](#)
[▶](#)
[◀](#)
[▶](#)
[Back](#)
[Close](#)
[Full Screen / Esc](#)
[Printer-friendly Version](#)
[Interactive Discussion](#)